








RESEARCH ARTICLE

Multiple mechanisms underpin cerebral and cerebellar white matter deficits in Friedreich ataxia: The IMAGE-FRDA study

Louisa P. Selvadurai¹  | Louise A. Corben^{1,2,3}  | Martin B. Delatycki^{2,3,4}  |
 Elsdon Storey⁵  | Gary F. Egan^{1,6}  | Nellie Georgiou-Karistianis¹  |
 Ian H. Harding¹ 

¹School of Psychological Sciences and Turner Institute for Brain and Mental Health, Monash University, Melbourne, Victoria, Australia

²Bruce Lefroy Centre for Genetic Health Research, Murdoch Children's Research Institute, Parkville, Victoria, Australia

³Department of Paediatrics, The University of Melbourne, Parkville, Victoria, Australia

⁴Victorian Clinical Genetics Services, Parkville, Victoria, Australia

⁵Department of Medicine, Monash University, Prahran, Victoria, Australia

⁶Monash Biomedical Imaging, Monash University, Clayton, Victoria, Australia

Correspondence

Nellie Georgiou-Karistianis, Turner Institute for Brain and Mental Health, School of Psychological Sciences, Monash University, Clayton Campus, Clayton, VIC 3800, Australia. Email: nellie.georgiou-karistianis@monash.edu

Funding information

National Health and Medical Research Council, Grant/Award Number: 1046037

Abstract

Friedreich ataxia is a progressive neurodegenerative disorder with reported abnormalities in cerebellar, brainstem, and cerebral white matter. White matter structure can be measured using in vivo neuroimaging indices sensitive to different white matter features. For the first time, we examined the relative sensitivity and relationship between multiple white matter indices in Friedreich ataxia to more richly characterize disease expression and infer possible mechanisms underlying the observed white matter abnormalities. Diffusion-tensor, magnetization transfer, and T1-weighted structural images were acquired from 31 individuals with Friedreich ataxia and 36 controls. Six white matter indices were extracted: fractional anisotropy, diffusivity (mean, axial, radial), magnetization transfer ratio (microstructure), and volume (macrostructure). For each index, whole-brain voxel-wise between-group comparisons and correlations with disease severity, onset age, and gene triplet-repeat length were undertaken. Correlations between pairs of indices were assessed in the Friedreich ataxia cohort. Spatial similarities in the voxel-level pattern of between-group differences across the indices were also assessed. Microstructural abnormalities were maximal in cerebellar and brainstem regions, but evident throughout the brain, while macroscopic abnormalities were restricted to the brainstem. Poorer microstructure and reduced macrostructural volume correlated with greater disease severity and earlier onset, particularly in peridentate nuclei and brainstem regions. Microstructural and macrostructural abnormalities were largely independent. Reduced fractional anisotropy was most strongly associated with axial diffusivity in cerebral tracts, and magnetization transfer in cerebellar tracts. Multiple mechanisms likely underpin white matter abnormalities in Friedreich ataxia, with differential impacts in cerebellar and cerebral pathways.

KEYWORDS

cerebellum, cerebrum, diffusion tensor imaging, Friedreich ataxia, magnetic resonance imaging, magnetization transfer imaging, volumetric imaging, white matter

Nellie Georgiou-Karistianis and Ian H. Harding are considered as joint senior author.

This is an open access article under the terms of the Creative Commons Attribution-NonCommercial-NoDerivs License, which permits use and distribution in any medium, provided the original work is properly cited, the use is non-commercial and no modifications or adaptations are made.

© 2020 The Authors. *Human Brain Mapping* published by Wiley Periodicals, Inc.

1 | INTRODUCTION

Friedreich ataxia (FRDA) is a recessively inherited disorder characterized by progressive movement incoordination, dysarthria, loss of reflexes, proprioceptive deficits, skeletal abnormalities, and cardiomyopathy (Delatycki & Corben, 2012). In 96% of cases FRDA is caused by homozygosity for a GAA repeat expansion in intron 1 of the *FXN* gene, leading to transcriptional repression of frataxin, a mitochondrial protein involved in iron regulation (Campuzano et al., 1996; Martelli & Puccio, 2014). Within the central nervous system, the most prominent pathology includes atrophy of the dorsal spinal tracts and cerebellar dentate nuclei (Pandolfo, 2008). Neuroimaging studies of cerebral gray and white matter demonstrate compelling evidence of abnormalities in cerebral structure (Della Nave, Ginestroni, Giannelli, et al., 2008; Rezende et al., 2016; Selvadurai et al., 2016), function (Dogan et al., 2016; Georgiou-Karistianis et al., 2012; Harding et al., 2016; Harding et al., 2017), and both intra-cerebral and cerebello-cerebral connectivity (Akhlaghi et al., 2011; Akhlaghi et al., 2014; Coccozza et al., 2018; Dogan et al., 2016; Harding et al., 2016; Rizzo et al., 2011; Zalesky et al., 2014). This body of evidence represents significant advances in the characterization of brain changes in individuals with FRDA. However, little is known about the mechanisms underlying widespread cerebro-cerebellar abnormalities or their significance to the FRDA phenotype. Addressing these knowledge gaps is critical if we are to discover new imaging biomarkers of disease severity and their relationship to clinical and functional outcomes for future clinical trials.

Interestingly in individuals with FRDA, widespread white matter deficits in cerebellar and cerebral tracts have been observed across a range of *in vivo* neuroimaging techniques. Firstly, diffusion tensor imaging studies have demonstrated widespread microstructural abnormalities across multiple measurements, including consistently reduced fractional anisotropy (FA), increased mean diffusivity (MD), and increased radial diffusivity (RD) (Akhlaghi et al., 2011; Akhlaghi et al., 2014; Della Nave, Ginestroni, Giannelli, et al., 2008; Della Nave et al., 2011; Dogan et al., 2016; Rezende et al., 2016; Rezende et al., 2019; Rizzo et al., 2011; Vavla et al., 2018; Vieira Karuta et al., 2015). The direction of changes in axial diffusivity has differed between studies (Akhlaghi et al., 2014; Della Nave et al., 2011; Rezende et al., 2016; Rezende et al., 2019; Vavla et al., 2018; Vieira Karuta et al., 2015). Microstructural abnormalities in the superior cerebellar peduncle (SCP) have also been identified using magnetization transfer imaging (Corben et al., 2014). Deficits are also evident at the macrostructural level, with reduced white matter volume reported in deep cerebellar white matter, brainstem, and frontal, cingulate, and anterior parietal regions (Della Nave, Ginestroni, Tessa, et al., 2008; França et al., 2009; Pagani et al., 2010; Rezende et al., 2016). Moreover, white matter indices show significant correlations with scores on clinical rating scales, GAA repeat length, age of disease onset, and disease duration (Rezende et al., 2016; Rizzo et al., 2011; Vavla et al., 2018). Furthermore, magnetic resonance spectroscopy (MRS) analysis has revealed metabolite abnormalities in cerebellar and cerebral white matter in FRDA (França et al., 2009; Gramegna et al., 2017; Iltis et al.,

2010). Together, these findings indicate that white matter disruption is a consistent correlate of disease expression in FRDA. However, it remains unclear which white matter indices are most sensitive to FRDA-related pathology, if they are differentially responsive to changes in different parts of the brain, and whether they reflect common or distinct pathological processes.

These questions can be addressed using comprehensive multi-modal neuroimaging of white matter in individuals with FRDA, including direct comparisons between the different available white matter indices. Although not direct measures of any specific property of individual axons, these measures have been associated with different types of white matter damage. While FA is considered sensitive but non-specific to multiple underlying neuropathological processes (Alexander et al., 2011), RD and the magnetization transfer ratio (MTR) may be influenced by axon myelination (Janve et al., 2013; Rausch et al., 2009), and changes in AD and volume loss have been associated with axonal damage (Sun et al., 2006) and degeneration (Salat, Kaye, & Janowsky, 1999), respectively. Comparison of deficits across multiple white matter indices may provide valuable information, albeit indirect (Jones, Knösche, & Turner, 2013), about the processes underpinning white matter changes in FRDA, which may be valuable for hypothesis-generation in future studies. Importantly, similar multi-modal approaches have provided new disease insights in other neurodegenerative disorders, including Huntington's disease (Poudel et al., 2015) and Alzheimer's disease (Canu et al., 2010; Huang, Friedland, & Auchus, 2007).

In the present study, we undertook a multi-modal assessment of the characteristics of whole-brain white matter in FRDA, as part of the IMAGE-FRDA study. We aimed to replicate previous white matter studies in a large single-site cohort of individuals with FRDA, by firstly characterizing the pattern of white matter abnormalities and secondly investigating their relationship with clinical variables. Furthermore, we aimed to extend the existing body of work by examining the relationships between white matter indices to determine whether different measures of white matter reflect common or unique disease-related processes in individuals with FRDA. Characterizing the pattern of observed alterations across multiple measures provides opportunities for novel insights into the potential mechanisms that drive white matter abnormalities across the brain (e.g., demyelination, axonal loss, volumetric loss).

2 | METHODS

2.1 | Participants

Data was collected as part of IMAGE-FRDA, a single-site longitudinal multi-modal neuroimaging study (Monash University, Melbourne, data collection 2013–2016) (Harding et al., 2016; Harding et al., 2017; Selvadurai et al., 2016). Data from 36 individuals with FRDA and 37 age- and gender-matched control participants were acquired for analysis. Five FRDA datasets were excluded after data collection due to diagnosed clinical depression ($n = 3$), in-scanner movement ($n = 1$)

and extensive brain atrophy ($n = 1$). One control dataset was excluded due to an image file error. Individuals with FRDA were genetically confirmed to be homozygous for a GAA repeat expansion in intron 1 of the *FXN* gene. These individuals had no comorbid neurological or psychiatric diagnoses based on clinical report. Eight individuals met criteria for late-onset FRDA (onset after 25 years of age; Lecocq et al., 2016). Onset age was defined as the age at which clinical symptoms of FRDA were first noticed by the individual or parents/carers. Disease severity was assessed by the full Friedreich ataxia rating scale (FARS; Subramony et al., 2005), scored out of 167, with higher scores indicating greater severity. Two individuals with FRDA had a diagnosis of diabetes. Table 1 shows participant demographic and clinical information.

All individuals provided informed, written consent to participate. All study procedures were approved by the Monash Health Human Research Ethics Committee.

2.2 | MRI data acquisition

Magnetic resonance images were acquired using a 3T Siemens Skyra Magnetic Resonance Scanner (Siemens, Erlangen, Germany) with a 32-channel head coil, located at Monash Biomedical Imaging, Melbourne.

Whole-brain T1-weighted images were acquired over 4 min and 26 s using a magnetization-prepared rapid gradient-echo sequence (MPRAGE), with 176 sagittal slices, voxel size $1 \times 1 \times 1 \text{ mm}^3$, matrix size = 256×256 , field of view = $256 \times 256 \text{ mm}^2$, echo time = 2.55 ms, and repetition time = 1,540 ms.

Whole-brain diffusion-weighted images were acquired over 13 min and 35 s using an echo-planar spin-echo sequence, with $b = 3,000$, 64 gradient directions, 60 axial slices, voxel size = $2.1 \times 2.1 \times 2.1 \text{ mm}^3$, matrix size = 122×122 , field of view = $256 \times 256 \text{ mm}^2$, echo time = 108 ms, and repetition time = 11.6 s.

For the magnetization transfer imaging, two whole-brain T2-weighted images were acquired over 4 min and 23 s each. One image was obtained following saturation with a magnetization transfer pulse (offset frequency = 1.2 kHz, gaussian envelope duration = 9.984 ms, flip angle = 500° , bandwidth = 192 Hz), and one without. Each image had 46 axial slices, voxel size = $0.9 \times 0.9 \times 3.0 \text{ mm}^3$, matrix size = 256×154 , field of view = $172.5 \times 230 \text{ mm}^2$, echo time = 8.4 ms, and repetition time = 734 ms.

2.3 | Diffusion tensor imaging (DTI)

Initial image processing utilized the FMRIB Diffusion Toolbox (FDT) from the FMRIB Software Library (FSL, Version 5.0.9; <https://fsl.fmrib.ox.ac.uk/fsl/fslwiki>; Smith et al., 2004). This included brain extraction (FSL-BET; Smith, 2002), correction for eddy currents (Andersson & Sotiropoulos, 2016), and fitting of diffusion tensors using DTIFIT (default linear regression algorithm; Behrens et al., 2003). Subsequent processing used the Diffusion Tensor Imaging ToolKit (DTI-TK, Version 2.3.1; <http://dti-tk.sourceforge.net>). The *fsl_to_dtitk* script converted FSL-generated eigenvalue maps into DTI-TK compatible DTI images.

Image registration was achieved using the tensor-based registration method described by Keihaninejad et al. (2013), providing improved tract alignment and sensitivity to group differences compared to scalar-based registration. Using DTI-TK, participants' DTI images were aligned to the group average space with affine and diffeomorphic registrations to form a group template (inter-subject registration). The group template was then aligned with the Illinois Institute of Technology DTI standard template (ICBM-152 space) using rigid, affine, and diffeomorphic registrations. Finally, the combined warps from the inter-subject and group-template-to-standard-template transformations were applied to the original DTI-TK images to normalize the data to ICBM-152 standard space. DTI-TK's Tensor Volume tool was subsequently used to calculate maps of FA, MD, AD,

TABLE 1 Demographic and clinical information for individuals with FRDA and healthy controls

| | FRDA ($n = 31$) | Controls ($n = 36$) | Statistic | p Value |
|------------------------------|---------------------------------|-------------------------------|--------------------|-----------|
| Demographic | | | | |
| Age (years) | 36.6 ± 13.0 (Range 18–63) | 36.5 ± 12.5 (Range 18–62) | $U = 536$ | .782 |
| Gender (M, F) | (17, 14) | (20, 16) | $\chi^2(1) = .003$ | .953 |
| Clinical data | | | | |
| BDI-II score | 8.2 ± 8.4 (Range 0–39) | 5.1 ± 5.8 (Range 0–24) | $U = 425$ | .093 |
| Age at disease onset (years) | 19.6 ± 8.8 (Range 6–40) | – | – | – |
| Disease duration (years) | 16.9 ± 9.5 (Range 5–48) | – | – | – |
| FARS score | 80.9 ± 28.4 (Range 19–126) | – | – | – |
| GAA1 repeat length | 546 ± 225 (Range 126–1,077) | – | – | – |
| GAA2 repeat length | 864 ± 253 (Range 215–1,293) | – | – | – |

Note: Mean \pm SD. GAA = number of GAA repeats in intron 1 of the *FXN* gene on the smaller (GAA1) and larger (GAA2) alleles. Abbreviations: BDI-II, Beck Depression Inventory II; FARS, Friedreich Ataxia Rating Scale; U , Mann-Whitney U -test; χ^2 , chi-square test.

and RD from the spatially normalized maps. Following this, all scalar maps were linearly registered to Montreal Neurological Institute (MNI) space with an affine transformation using FSL FLIRT (Jenkinson, Bannister, Brady, & Smith, 2002), with the MNI152_T1_1mm_brain template as the registration target.

2.4 | Magnetization transfer imaging (MTI)

For each participant, the T2 image acquired with saturation by a magnetization transfer pulse (MT) and the T2 image acquired without saturation (MT₀) were brain-extracted (FSL-BET). The MT image was then linearly registered to the MT₀ image (FSL-FLIRT with seven degrees of freedom). The Magnetization Transfer Ratio (MTR) at each image voxel was calculated as follows:

$$\frac{MT_0 - MT}{MT_0} \times 100$$

The MTR maps were linearly co-registered to the unregistered DTI images using a rigid body transformation with six degrees of freedom. The maps were then warped to ICBM-152 standard space by applying the inter-subject and group-template-to-standard-template deformation fields obtained from the tensor-based registration of the DTI images. Finally, the images were warped to MNI space by applying the same transformation used for registration of the DTI images to MNI space described above.

2.5 | Volumetric tensor-based morphometry (TBM)

TBM maps (Ashburner & Friston, 2000) were generated using Statistical Parametric Mapping software, version 12 (SPM12; <http://www.fil.ion.ucl.ac.uk/spm/>) and the Computational Anatomy Toolbox (CAT12; <http://www.neuro.uni-jena.de/cat/>). The T1-weighted images were first bias-corrected and segmented by tissue class using the machinery and tissue probability maps of SPM12 to produce gray and white matter partial-volume images for each subject. These images were subsequently nonlinearly warped to the IXI555_MNI152 gray and white matter templates, respectively, using DARTEL registration implemented in CAT12 (Ashburner, 2007). The Jacobian determinant of the warp field defining the nonlinear registration from native to standard space was subsequently written out, providing a map in MNI space of the local volume at each voxel in the brain, agnostic to tissue classification, for each individual. All processes were implemented using default CAT12 (r1363) segmentation parameters, with the additional option of writing out Jacobian determinant maps in standard space. Masking, smoothing, and statistical analysis processes are described below.

2.6 | White matter masking

The FA, MD, AD, RD, MTR, and volume maps in MNI space were masked to only include white matter regions based on an automated

segmentation of the FSL MNI152_T1_1mm_brain standard template using FMRIB's Automated Segmentation Tool (FAST; Zhang, Brady, & Smith, 2001) with a three-tissue class binary segmentation (see Figure S1). Each map was smoothed with a 1 mm FWHM Gaussian smoothing kernel within the white matter mask, as per Klauer et al. (2017).

2.7 | Statistical analyses

Cluster-level between-group differences for each white matter metric across all six indices (FA, MD, AD, RD, MTR, volume) were assessed using FSL's nonparametric *randomize* tool (Winkler, Ridgway, Webster, Smith, & Nichols, 2014) (see below for inference details for all *randomize* analyses). Age and gender were included as covariates of non-interest. Furthermore, each microstructural metric (FA, MD, AD, RD, and MTR) was orthogonalised with respect to volume when conducting the between-group analyses, in order to infer differences in microstructural measurements independently of any volumetric differences between the groups.

Furthermore, among the FRDA group, linear relationships between the six white matter indices and (a) disease severity (FARS score), (b) GAA1 repeat length, and (c) age of disease onset were also evaluated using *randomize*. Given a strong correlation between the FARS score and disease duration ($r = .640, p < .001$), disease duration was not used as a correlate to avoid redundancy. White matter metric maps for each FRDA participant were first corrected for the effect of healthy aging: for each metric, the linear relationship with participant age was first calculated for the control group at each voxel. Data from each participant in the FRDA group was then adjusted to the mean age of the sample. FA, MD, AD, RD, and MTR maps were not orthogonalised with respect to volume here, in order to evaluate the relationship of each independent metric against clinical variables.

Two analyses were conducted to investigate relationships between different white matter indices. Specifically, the relationship between changes in FA (a sensitive but nonspecific metric reflecting properties of tissue microstructure) was compared to changes in measures that may be related to more specific white matter tissue properties (AD, RD, MTR, and volume). The purpose of these analyses was to examine the dependencies between FA and the other metrics; as such, the microstructural metrics were not orthogonalised with respect to volume.

The first analysis investigated whether the spatial overlap of *between-group differences* was a result of shared variance between FA and the other indices, or representative of independent effects, by correlating the indices within the FRDA group. A mask was created representing the spatial intersection of significant FA differences and significant differences in the second metric (AD, RD, MTR, or volume). Within the masked region, the Pearson correlation between FA and the second metric was estimated at each voxel across participants in the FRDA cohort. Inference was conducted using *randomize*.

The second analysis considered between-group differences in FA versus AD, RD, MTR, and volume at each white matter voxel, regardless of statistical significance. Spatial correlations were performed to investigate the covariation of these differences across voxels, and to

examine whether patterns of covariation differed across different white matter regions. Six white matter regions-of-interest (ROIs) were selected: the superior, middle, and inferior cerebellar peduncles, corticospinal tracts, superior longitudinal fasciculi, and splenium of the corpus callosum. All ROIs showed between-group differences across at least two indices. Additionally, the three pairs of cerebellar peduncles are of particular interest in FRDA as a cerebellar disorder, and there is previous MRI evidence of disruption to these pathways, most consistently in the superior cerebellar peduncle (Selvadurai et al.,

2018). Furthermore, the corticospinal tracts are implicated in FRDA given the pyramidal weakness and extensor plantar reflexes forming part of the clinical picture, previous evidence of disruption across multiple diffusion metrics, and evidence of loss of Betz cells at the cortical termination of the tract (Koeppen & Makurkiewicz, 2013; Parkinson et al., 2013; Selvadurai et al., 2018). The superior longitudinal fasciculus was selected as a representative association tract due to consistent evidence of between-group differences across the metrics in the current analysis (differences were found in FA, MD, AD, and RD). The

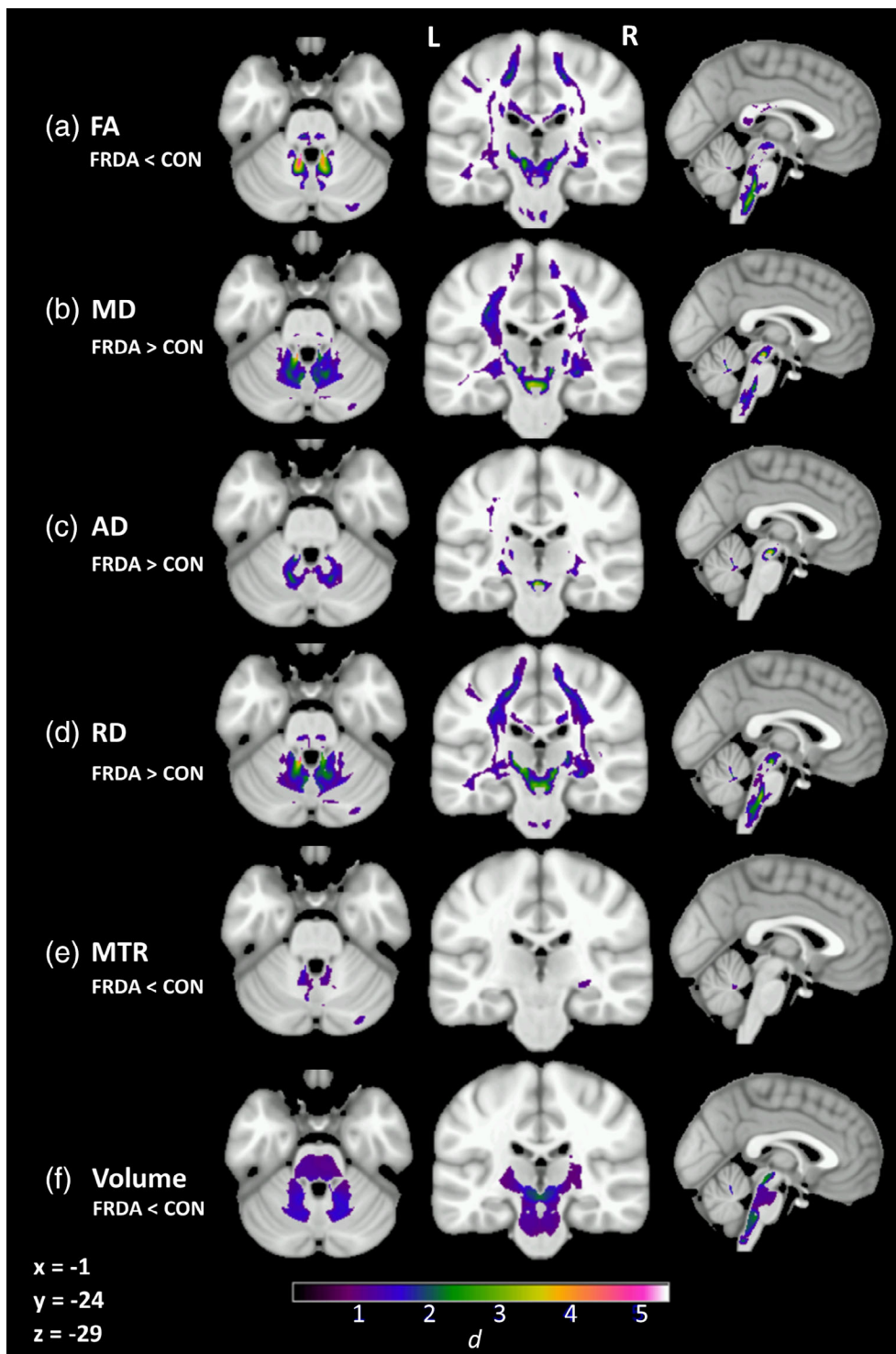


FIGURE 1 Significant group-level differences between individuals with FRDA and controls (cluster-level FWE-corrected $p < .05$) in (a) fractional anisotropy (FA), (b) mean diffusivity (MD), (c) axial diffusivity (AD), (d) radial diffusivity (RD), and (e) magnetization transfer ratio (MTR) after accounting for (f) volume. Cohen's d indicated by color gradient

TABLE 2 Anatomical location and effect sizes (Cohen's *d*) of group differences in white-matter metrics

| Region | FA | | MD | | AD | | RD | | MTR | | Volume | |
|--------------------|---|---|------------|--|------------|--|------------|--|------------|--|------------|--|
| | FRDA < CON | | FRDA > CON | | FRDA > CON | | FRDA < CON | | FRDA < CON | | FRDA < CON | |
| Cerebellar tracts | Peri-dentate white matter | ■ | ■ | | | | | | | | | |
| | Superior cerebellar peduncle | | ■ | | | | | | | | | |
| | Middle cerebellar peduncle | | ■ | | | | | | | | | |
| Projection tracts | Inferior cerebellar peduncle | | ■ | | | | | | | | | |
| | Corticospinal tract | | ■ | | | | | | | | | |
| | Anterior thalamic radiation | | ■ | | | | | | | | | |
| Commissural tracts | Posterior thalamic radiation | | ■ | | | | | | | | | |
| | Peri-thalamic WM | | ■ | | | | | | | | | |
| | Corpus callosum (genu) | | ■ | | | | | | | | | |
| Association tracts | Corpus callosum (body) | | ■ | | | | | | | | | |
| | Corpus callosum (splenium) | | ■ | | | | | | | | | |
| | Superior longitudinal fasciculus | | ■ | | | | | | | | | |
| | Inferior longitudinal fasciculus/ Inferior fronto-occipital fasciculus (posterior region) | | ■ | | | | | | | | | |
| | Uncinate fasciculus | | ■ | | | | | | | | | |
| Fornix | | ■ | | | | | | | | | | |
| Cingulum | | ■ | | | | | | | | | | |

Note: □ (*d* = 0.5–0.99) ■ (*d* = 1–1.99) ■ (*d* = 2–2.99) ■ (*d* = 3–3.99) ■ (*d* = 4+).

Abbreviations: AD, axial diffusivity; FA, fractional anisotropy; MD, mean diffusivity; MTR, magnetization transfer ratio; RD, radial diffusivity.

splenium of the corpus callosum was selected as a representative commissural tract as it showed between-group differences across three metrics and longitudinal changes have been reported in a previous study of FRDA (Mascalchi et al., 2016). A seventh ROI, the genu of the corpus callosum, was included as it did *not* show significant differences in white matter indices between the FRDA and control groups. ROIs were defined by the van Baarsen et al. (2016) cerebellar atlas, the John Hopkins University (JHU) probabilistic white matter atlas (Hua et al., 2008), and the ICBM-DTI-81 white matter labels (Oishi et al., 2008) (see Figure S2). For each of the six white matter indices, the size of the between-group difference in that index (FRDA group mean – control group mean) was calculated at each ROI voxel. Across all voxels within each ROI, between-group differences in FA were correlated with between-group differences in AD/RD/MTR/volume, using Pearson correlations (SPSS Statistics v. 24).

All *randomize* analyses consisted of 5,000 permutations for each contrast. Whole-brain voxel-wise correction for multiple comparisons was achieved using cluster-based inference (Forman et al., 1995), with a cluster-forming threshold (uncorrected) of $p < 0.001$ and a cluster-level significance threshold (family-wise error corrected) of $p < 0.05$.

3 | RESULTS

3.1 | Between-group differences

Significant between-group differences between individuals with FRDA and controls across the six white matter indices (FA, MD, AD, RD, MTR, volume) are displayed in Figure 1. Additionally, Cohen's *d* was calculated at each brain voxel. For each major white matter region (defined by the van Baarsen, JHU, and ICBM-DTI-81 atlases), the effect sizes across voxels within the region were extracted. The highest observed Cohen's *d* effect size value in each region is presented in Table 2. See Table S1 for a formal tabulation of cluster-level results.

Robust between-group differences in all indices (Cohen's $d > 1$) were evident throughout the cerebellar white matter and tracts, particularly adjacent to the dentate nuclei and in the SCP. Abnormalities in all diffusion indices (FA, MD, AD, RD) and volume were also evident in the cortico-spinal tracts and peri-thalamic region, indicating disruption across the full length of the cerebello-thalamo-cerebral pathways in individuals with FRDA, compared to controls. More circumscribed abnormalities were also evident in long association fibers, and posterior aspects of the corpus callosum in individuals with FRDA, compared to controls. All between-group differences were consistent with poorer white matter status in the FRDA group, with the exception of decreased AD in the splenium of the corpus callosum (not displayed here; see Table S1).

3.2 | Clinical correlations

Significant correlations among individuals with FRDA were found between disease severity (FARS score) and FA, MD, AD, RD, and volume. These occurred most robustly and consistently in peri-dentate

regions (Figure 2; Table S2). More sporadic correlations were evident in brainstem and subcortical regions for each metric.

Significant correlations were also found between the age of disease onset and each of MD, AD, RD, and MTR (Figure 2; Table S3), most consistently in brainstem regions. In addition, the repeat length of GAA1 correlated with volume within the inferior cerebellar peduncle (not depicted; Table S3 and Figure S3).

3.3 | Between-index comparisons

3.3.1 | Correlations between index values across individuals with FRDA

The first between-index analysis was conducted within white matter areas where a between-group difference was observed in both FA and another metric. Correlations at the cluster-level revealed significant associations between FA and each of AD and MTR in the peridentate/SCP, and between FA and RD in multiple regions throughout the white matter mask (Figure 3, Table S4). No significant correlations were found between FA values and volume, suggesting that overlapping microstructural and macrostructural changes were not strongly associated.

3.3.2 | Spatial correlations across voxels

The second between-index analysis investigated covariance in the between-group differences in metrics across white matter voxels. Figure 4 illustrates the group FA difference in each voxel plotted against the group difference for each of AD, RD, MTR and volume, in the seven white matter ROIs. A number of patterns were observed. In particular, group differences in RD correlated strongly with those in FA across all regions, while the strength of the correlation between the FA group differences and group differences in the other indices varied between regions. Specifically, the AD group differences showed correlations with the FA differences in the cerebral tracts but not the cerebellar peduncles. The MTR differences correlated with the FA differences in the cerebellar peduncles and the corpus callosum but not strongly in other tracts. The volume group differences showed a medium-sized correlation with FA differences in the corticospinal tract and middle cerebellar peduncle only.

4 | DISCUSSION

This study reports widespread disruption to cerebello-cerebral and intracerebral white matter pathways in individuals with FRDA. For the first time, we have comprehensively documented these alterations across multiple microstructural white matter measurements as well as macrostructural volumetric measurements. Consistent with previous studies (Akhlaghi et al., 2011; Corben et al., 2014), the observed abnormalities were maximal in the SCP, particularly adjacent to the

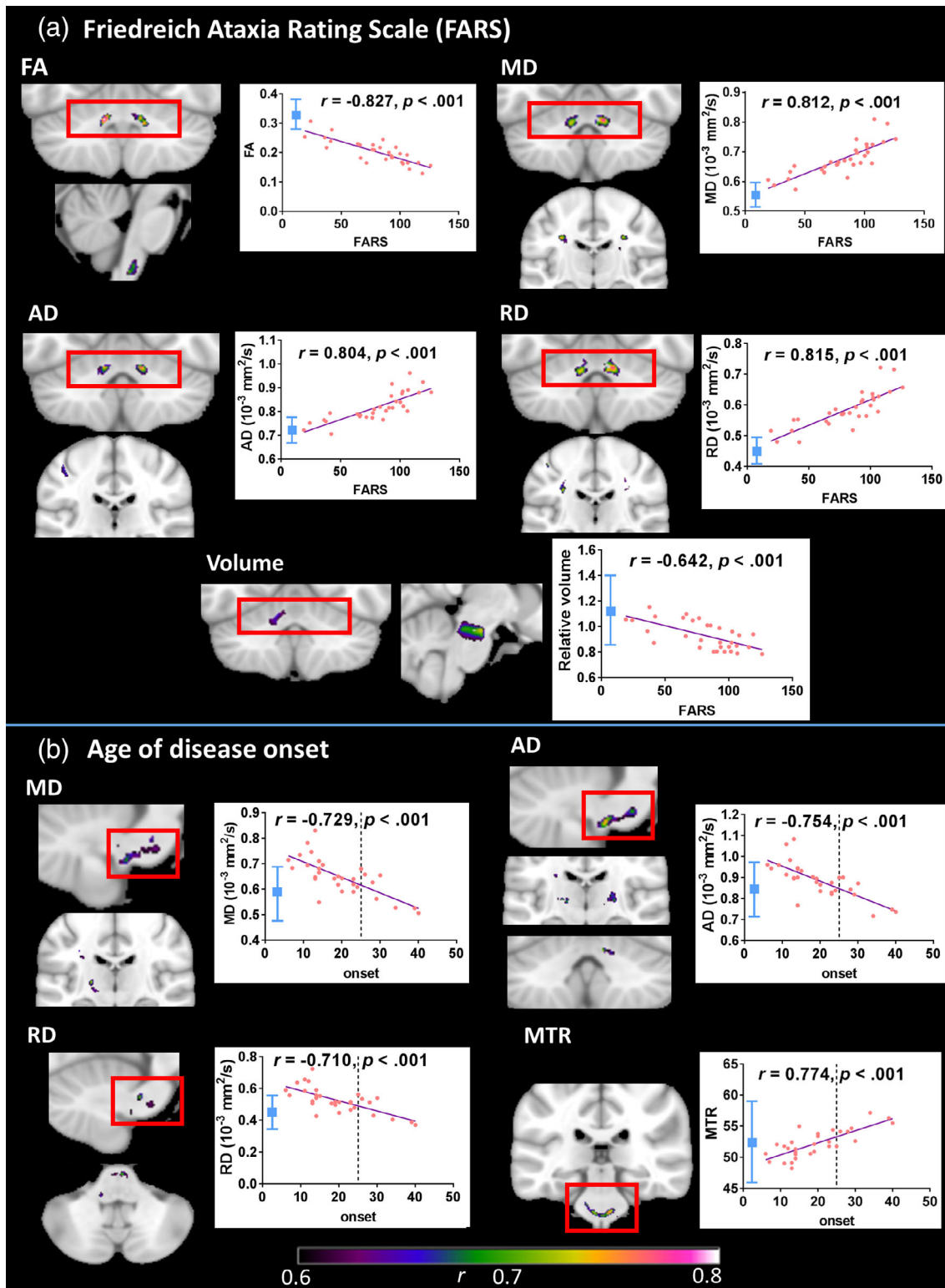


FIGURE 2 Correlations between white matter indices and FARS scores/age of disease onset (cluster-level FWE-corrected $p < .05$) where effect size (r , indicated by color gradient) is greater than 0.6. Scatterplots display correlations between FARS score/age of onset and mean value within indicated region. Line $x = 25$ (onset) indicates cut-off for late-onset FRDA. Control mean ± 2 SD in blue. Images are displayed in neurological space (left hemisphere on left). AD, axial diffusivity; FA, fractional anisotropy; MD, mean diffusivity; MTR, magnetization transfer ratio; RD, radial diffusivity

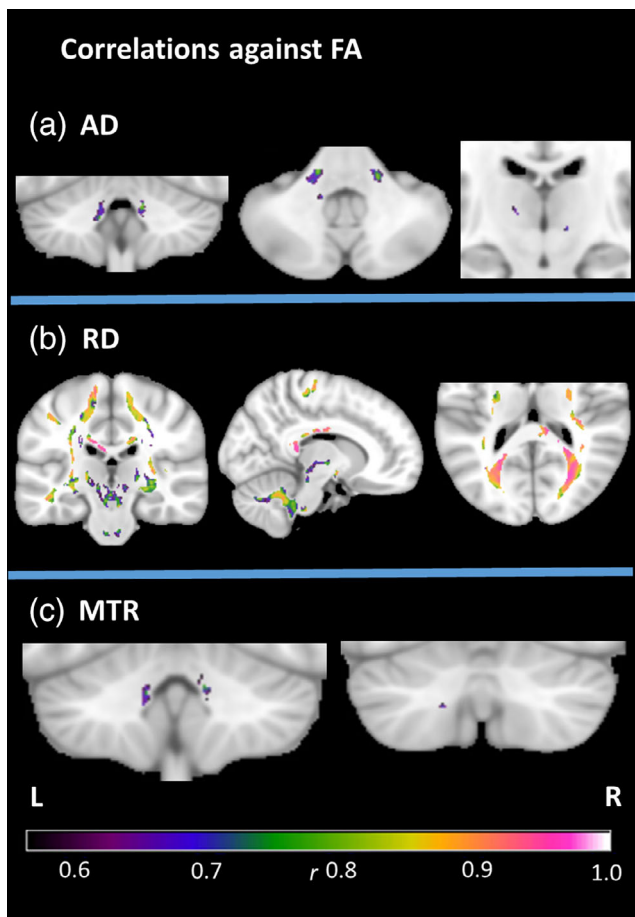


FIGURE 3 Between-metric correlations in the FRDA group at cluster-level FWE-corrected $p < .05$, with the mask defined by the intersection of significant group differences in FA and the named metric. Effect sizes (r) indicated by color gradient. AD, axial diffusivity; FA, fractional anisotropy; MTR, magnetization transfer ratio; RD, radial diffusivity

dentate nuclei, where white matter status was strongly correlated with clinical indices. Comparisons between the indices provided indirect support for multiple independent neuropathological processes, with spatially overlapping microstructural (diffusion) and macrostructural (volume) alterations manifesting independently. Moreover, we provide preliminary evidence for a distinction between the nature of the underlying tissue disruption predominating in affected cerebellar pathways on one hand, and cerebral tracts on the other. The results indicate that different white matter measurements may be independently sensitive to distinct disease processes in FRDA.

4.1 | White matter abnormalities in FRDA

Significant differences in all six white matter indices were evident in individuals with FRDA relative to controls. The direction of these effects were indicative of white matter disruption as observed in other progressive neurological disorders, including *lower* FA, *higher*

MD, AD, and RD (Alcauter, Barrios, Díaz, & Fernández-Ruiz, 2011; Rosas et al., 2010), *lower* MTR (Tambasco et al., 2015), and *decreased* white matter volume (Tabrizi et al., 2009) relative to healthy controls. Interestingly, we found *decreased* AD, restricted to the splenium of the corpus callosum. It is notable that both increases (Della Nave et al., 2011; Vavla et al., 2018) and decreases (Rezende et al., 2016; Vieira Karuta et al., 2015) in AD have been reported in previous FRDA studies. This finding was collocated with reduced FA and increased RD, providing corroborative evidence as to the importance of white matter aberrations in the splenium; however, the interpretation of the direction of this effect is currently unclear.

Importantly, we show for the first time that group differences in diffusivity-based indices (FA, MD, AD, and RD) and MTR occurred over and above any white matter volume loss. Similar findings have been observed in Alzheimer's disease, indicating that diffusion indices are sensitive to white-matter disruption beyond volume deficits (Canu et al., 2010).

Different white matter indices were differentially impacted by FRDA. Microstructural abnormalities (DTI) showed the largest effect sizes relative to controls. These changes were widespread, but particularly evident in the SCP and corticospinal tracts. This pattern largely corroborates previous reports in FRDA (Della Nave et al., 2011; Rezende et al., 2016; Vieira Karuta et al., 2015). More circumscribed evidence of MTR abnormalities was also found in the SCP, although effect sizes were smaller relative to the co-localized DTI group differences. This finding is consistent with one previous study in FRDA which also reported reduced MTR in the SCP but not in the genu of the corpus callosum (Corben et al., 2014). Finally, macrostructural abnormalities (reduced white matter volume) were also evident throughout cerebellar white matter and cerebello-thalamic pathways, replicating reports of reduced volume in deep cerebellar white matter (Della Nave, Ginestroni, Giannelli, et al., 2008) and reduced size of the SCP (Akhlaghi et al., 2011; Pagani et al., 2010). Conversely, the current findings are inconsistent with previous reports of reduced white matter within frontal, cingulate, and parietal areas in addition to cerebellar regions (França et al., 2009; Rezende et al., 2016). These distinctions may relate to the less conservative false discovery rate correction used for multiple comparisons in these latter studies (Verhoeven, Simonsen, & McIntyre, 2005), or may reflect unknown cohort-specific effects.

Taken together, the pattern of between-group effects across white matter imaging modalities indicate that the most spatially consistent and largest absolute effects occur in the cerebello-thalamo-cerebral pathways. Between-group differences in white matter indices were particularly distinct in FA, MD, and RD within the SCP immediately adjacent to the dentate nuclei (Figure 2; e.g., FA values in all but two individuals with FRDA were more than two standard deviations below the control data in this region). These effects implicate the dentatofugal white matter pathways as key sites of aberration in FRDA, consistent with neuropathological findings of atrophy of the dentate nucleus, its white matter projections, and the superior cerebellar peduncle at the level of the brainstem (Koeppen & Mazurkiewicz, 2013). Furthermore, diffusion indices in the peri-dentate region were

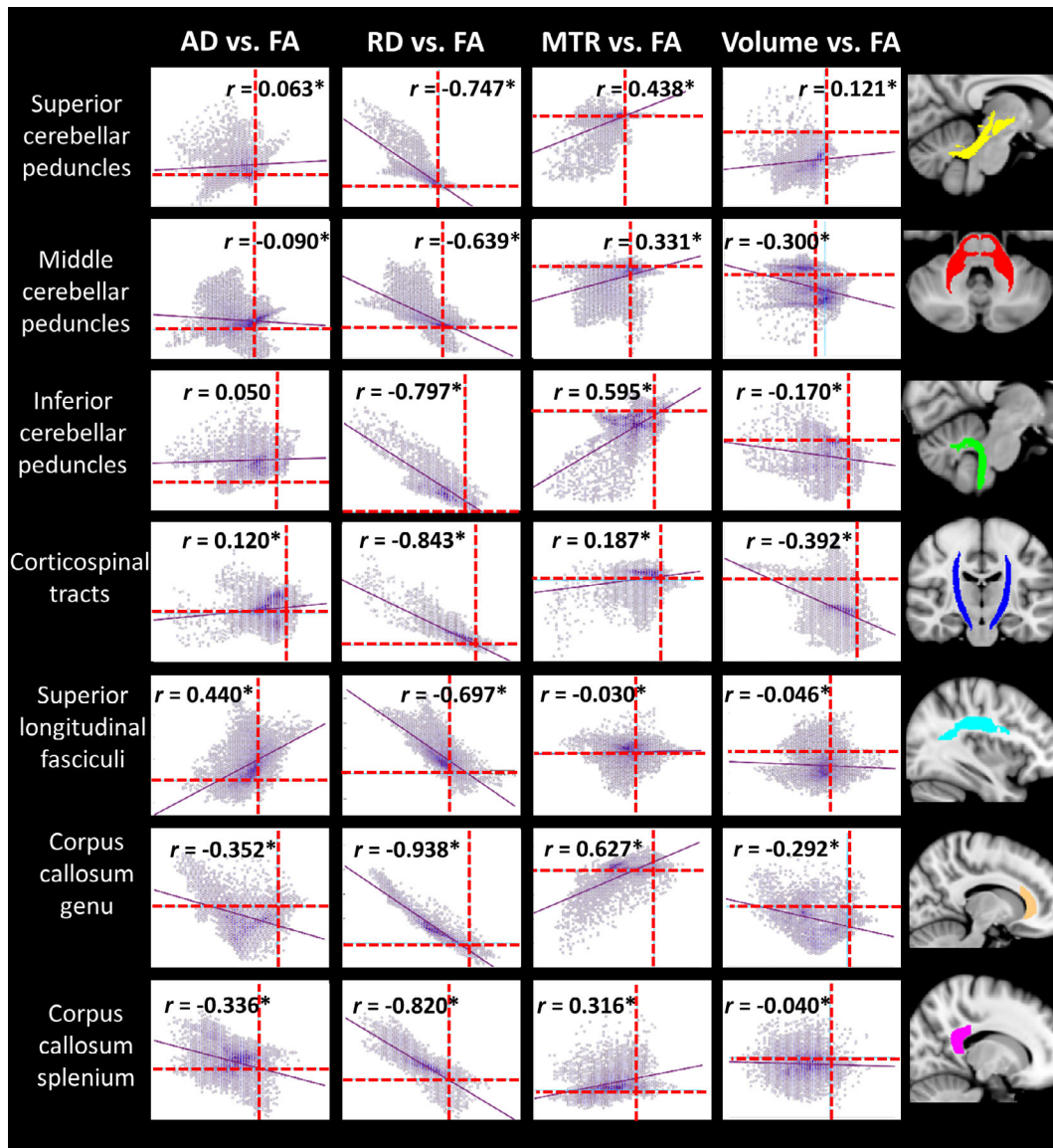


FIGURE 4 Pearson correlations for between-group differences in FA versus AD/RD/MTR/volume in each voxel within regions-of-interest. Dotted lines represent $x = 0$ and $y = 0$. FA is plotted on x-axis, comparison indices on y-axis. *Significant at corrected $p < .05$, accounting for 28 comparisons (i.e., $p < .002$). AD, axial diffusivity; FA, fractional anisotropy; MTR, magnetization transfer ratio; RD, radial diffusivity

also very highly correlated with disease severity (up to $r = 0.82$), corroborating previous findings and indicating a strong association of peri-dentate white matter aberrations with the phenotypic expression, and potentially progression, of FRDA (Della Nave, Ginestroni, Tessa, et al., 2008; Pagani et al., 2010; Rezende et al., 2016).

Consistent between-group differences were also observed in cerebral regions of the cortico-spinal tracts, with correlations additionally observed between diffusion indices in this region and both disease severity and age of disease onset. This complements known loss of Betz cells in the motor cortex and degeneration in the spinal regions of these tracts (Koeppen & Mazurkiewicz, 2013; Pandolfo, 2008). However, abnormalities were also observed in white matter pathways not linked to known areas of pathology, such as the splenium of the corpus callosum. Moreover, repeat length on the

smaller allele (GAA1), which has been shown to directly influence the expression of frataxin (Clark et al., 2018), correlated negatively with white matter volume in the inferior cerebellar peduncle/medulla area. These observations raise the possibility that some cerebral white matter aberrations result from a primary effect of frataxin deficiency. Further work is necessary to disambiguate primary and secondary disease-related effects.

The current between-group results may reflect degenerative processes, developmental processes (i.e., incomplete development of white matter), or both. Indeed, recent histological evidence indicates that neuropathology in FRDA involves areas of hypoplasia as well as areas of degeneration (Koeppen, Becker, Qian, & Feustel, 2017), and a recent neuroimaging study indicated that children and adults with FRDA show different patterns of white and gray matter abnormalities

across the cerebrum, brainstem, and spinal cord (Rezende et al., 2019). Interestingly, our results showed that within the cerebrum, significant correlations with onset age (which may represent developmental components of the disease course) tended to cluster in perithalamic regions, while correlations with disease severity (which may reflect degenerative components) tended to occur more superiorly. In the brainstem and cerebellum, correlations with onset age were evident in the pons, while associations with disease severity were more consistently found in peri-dentate regions. Notably, recent neuropathological evidence suggests that spinal cord pathology in FRDA results from compromised development, whereas dentate pathology reflects degeneration (Koeppen et al., 2017; Koeppen, Ramirez, Becker, Feustel, & Mazurkiewicz, 2015). However, our observation of sub-threshold age of onset correlations in peri-dentate regions cautions against interpreting onset and severity correlations as exclusively impacting different brain regions. Rather, these findings indicate that both developmental and degenerative processes may occur in brain white matter in FRDA, although whether these processes target particular tracts requires longitudinal follow-up of pediatric cohorts.

4.2 | Multiple white matter pathologies in FRDA

In previous FRDA white matter studies, it has been unclear whether co-localized significant differences in two or more indices are the result of common or distinct pathological processes. The present results indicate extensive shared variance *across individuals* between FA and RD measurements, alongside relatively less shared variance between FA and AD/MTR, and largely independent FA and volume effects. Taken together, these findings suggest that FA, AD, MTR, and volume may each provide unique and complementary information in FRDA, with the spatial overlap of between-group differences possibly representing co-occurrence of independent pathological processes - for example, white matter volume loss *and* abnormal white matter microstructure. Furthermore, the strong shared variance between FA and RD may indicate that they reflect similar underlying properties of the white matter (consistent with findings that FA and RD have a high level of shared genetic variance; Hatton et al., 2018), which likely explains their striking overlap in the between-group differences shown here and in previous work (e.g., Rezende et al., 2016). As such, it may be pertinent to be cautious in interpreting FA and RD effects as separate and additive lines of evidence regarding white matter abnormalities in FRDA.

Furthermore, we investigated covariation of *disease effects* (i.e., between-group differences) using a voxel-based approach in major white matter regions. Group differences in FA and RD were highly correlated across voxels suggesting they may reflect a common underlying disease process. On the other hand, MTR group differences correlated most consistently with FA group differences in cerebellar tracts, while correlations between AD and FA group differences were most evident in cerebral tracts. A speculative interpretation of this pattern, for further investigation in histological and preclinical studies, is that cerebellar peduncle disruptions are more weighted

toward myelin deficits, while cerebral disruptions are more strongly associated with axonal pathology. This distinction might then contribute to the proposed model of primary cerebellar and secondary cerebral degeneration in the cerebello-thalamo-cerebral pathways. Whereas primary cerebellar white matter disruption may be driven by demyelination secondary to frataxin loss, consistent with *in vitro* work showing that frataxin deficits disrupt peripheral myelinating cells (Lu et al., 2009), secondary cerebral white matter disruption may result from subsequent changes to axonal integrity. Investigation of this potential disease process will require further research but may provide important information as to the mechanisms and progression of white matter disruption in FRDA.

4.3 | Limitations and future directions

Several limitations must be considered. While diffusion tensor imaging is a well-accepted measure of white matter characterization, definitive interpretation of indices with regard to underlying biological mechanisms must be approached with caution, as changes in indices can result from a number of different biological processes (Jones et al., 2013; Wheeler-Kingshott & Cercignani, 2009). While this study provides a model of both shared and unique pathological processes driving primary and secondary white matter deficits in FRDA, histological or cellular corroboration is necessary.

Furthermore, interpretations regarding associations between disease severity across individuals (as an indicator of disease progression) and white matter indices are limited by our cross-sectional design. Longitudinal investigations are essential to understand the impact of disease progression, and to disambiguate developmental versus degenerative white matter changes in FRDA.

It should also be noted that alterations in brain white matter have been observed among individuals with Type I and Type II diabetes (Moghaddam, Sherbaf, & Aarabi, 2019; Yoon et al., 2018). The present analyses included two individuals with diabetes. Although their inclusion did not unduly influence the overall pattern of results (see Figure S5), these individuals were in the lower extremes of the distribution of FA values within the FRDA group (see Figure S4). However, these participants also had relatively long disease durations and high FARS scores, which precludes differentiation between the effects of diabetes and progressed disease in this case. The effects seen here highlight the relevance of considering the impact of diabetes in future studies, particularly as diabetes prevalence is reported as high as 30% in some cohorts (Delatycki & Corben, 2012).

Finally, the finding that disease severity preferentially correlated with white matter indices in *peri-dentate* areas does not necessarily preclude the relevance of other white matter tracts to the FRDA phenotype. The FARS score particularly reflects impairment of cerebellar function (Delatycki, 2009). Further investigation of correlations between white matter indices and alternative cognitive, affective, or behavioral measures may be required to determine the clinical significance of white matter abnormalities.

Our findings indicate that widespread white matter deficits in FRDA likely result from multiple pathophysiological processes, to which different magnetic resonance imaging based white matter indices are differentially sensitive. This work provides important advances contributing to a detailed model of the neuropathological profile of FRDA, and motivates comprehensive longitudinal investigations to understand and track the association between white matter disruption and clinical progression.

ACKNOWLEDGMENTS

The IMAGE-FRDA study was funded by the Australian National Health and Medical Research Council (Project Grant 1046037). The authors thank the individuals with Friedreich ataxia and the control participants who took part in the study, and Monique Stagnitti for participant recruitment and scanning.

CONFLICT OF INTEREST

The authors declare no potential conflict of interest.







AUTHOR CONTRIBUTIONS

L.P.S. conducted statistical analyses and wrote the manuscript. L.A.C. conceptualized the project and reviewed, critiqued, and edited the manuscript. M.B.D. conceptualized the project and reviewed, critiqued, and edited the manuscript. E.S. conceptualized the project and reviewed the manuscript. G.F.E. conceptualized the project and reviewed, critiqued, and edited the manuscript. N.G-K. conceptualized the project and reviewed, critiqued, and edited the manuscript. I.H.H. conducted statistical analyses and reviewed, critiqued, and edited the manuscript.

DATA AVAILABILITY STATEMENT

The data that support the findings of this study are available on request from the corresponding author. The data are not publicly available due to privacy or ethical restrictions.

ORCID

Louisa P. Selvadurai  <https://orcid.org/0000-0003-3840-9736>
 Louise A. Corben  <https://orcid.org/0000-0001-8767-4582>
 Martin B. Delatycki  <https://orcid.org/0000-0002-8769-2569>
 Elsdon Storey  <https://orcid.org/0000-0001-5887-3267>
 Gary F. Egan  <https://orcid.org/0000-0002-3186-4026>
 Nellie Georgiou-Karistianis  <https://orcid.org/0000-0003-0718-6760>
 Ian H. Harding  <https://orcid.org/0000-0002-6843-9592>

REFERENCES

- Akhlaghi, H., Corben, L., Georgiou-Karistianis, N., Bradshaw, J., Storey, E., Delatycki, M. B., & Egan, G. F. (2011). Superior cerebellar peduncle atrophy in Friedreich's ataxia correlates with disease symptoms. *The Cerebellum*, 10(1), 81–87. <https://doi.org/10.1007/s12311-010-0232-3>
- Akhlaghi, H., Yu, J., Corben, L., Georgiou-Karistianis, N., Bradshaw, J. L., Storey, E., ... Egan, G. F. (2014). Cognitive deficits in Friedreich ataxia correlate with micro-structural changes in dentatorubral tract. *The Cerebellum*, 13(2), 187–198. <https://doi.org/10.1007/s12311-013-0525-4>
- Alcauter, S., Barrios, F. A., Díaz, R., & Fernández-Ruiz, J. (2011). Gray and white matter alterations in spinocerebellar ataxia type 7: An in vivo DTI and VBM study. *NeuroImage*, 55(1), 1–7. <https://doi.org/10.1016/j.neuroimage.2010.12.014>
- Alexander, A. L., Hurley, S. A., Samsonov, A. A., Adluru, N., Hosseinbor, A. P., Mossahebi, P., ... Field, A. S. (2011). Characterization of cerebral white matter properties using quantitative magnetic resonance imaging stains. *Brain Connectivity*, 1(6), 423–446. <https://doi.org/10.1089/brain.2011.0071>
- Andersson, J. L. R., & Sotiropoulos, S. N. (2016). An integrated approach to correction for off-resonance effects and subject movement in diffusion MR imaging. *NeuroImage*, 125, 1063–1078. <https://doi.org/10.1016/j.neuroimage.2015.10.019>
- Ashburner, J. (2007). A fast diffeomorphic image registration algorithm. *NeuroImage*, 38(1), 95–113. <https://doi.org/10.1016/j.neuroimage.2007.07.007>
- Ashburner, J., & Friston, K. J. (2000). Voxel-based morphometry—the methods. *NeuroImage*, 11(6), 805–821. <https://doi.org/10.1006/nimg.2000.0582>
- Behrens, T. E. J., Woolrich, M. W., Jenkinson, M., Johansen-Berg, H., Nunes, R. G., Clare, S., ... Smith, S. M. (2003). Characterization and propagation of uncertainty in diffusion-weighted MR imaging. *Magnetic Resonance in Medicine*, 50(5), 1077–1088. <https://doi.org/10.1002/mrm.10609>
- Campuzano, V., Montermini, L., Moltò, M. D., Pianese, L., Cossée, M., Cavalcanti, F., ... Pandolfo, M. (1996). Friedreich's ataxia: Autosomal recessive disease caused by an intronic GAA triplet repeat expansion. *Science*, 271(5254), 1423–1427. <https://doi.org/10.1126/science.271.5254.1423>
- Canu, E., McLaren, D. G., Fitzgerald, M. E., Bendlin, B. B., Zoccatelli, G., Alessandrini, F., ... Frisoni, G. B. (2010). Microstructural diffusion changes are independent of macrostructural volume loss in moderate to severe Alzheimer's disease. *Journal of Alzheimer's Disease*, 19(3), 963–976. <https://doi.org/10.3233/JAD-2010-1295>
- Clark, E., Johnson, J., Dong, Y. N., Mercado-Ayon, E., Warren, N., Zhai, M., ... Lynch, D. R. (2018). Role of frataxin protein deficiency and metabolic dysfunction in Friedreich ataxia, an autosomal recessive mitochondrial disease. *Neuronal Signaling*, 2(4), NS20180060. <https://doi.org/10.1042/ns20180060>
- Cocozza, S., Costabile, T., Tedeschi, E., Abate, F., Russo, C., Liguori, A., ... Saccà, F. (2018). Cognitive and functional connectivity alterations in Friedreich's ataxia. *Annals of Clinical and Translational Neurology*, 5(6), 677–686. <https://doi.org/10.1002/acn3.555>
- Corben, L. A., Kashuk, S. R., Akhlaghi, H., Jamadar, S., Delatycki, M. B., Fielding, J., ... Egan, G. F. (2014). Myelin paucity of the superior cerebellar peduncle in individuals with Friedreich ataxia: an MRI magnetization transfer imaging study. *Journal of the Neurological Sciences*, 343(1), 138–143. <https://doi.org/10.1016/j.jns.2014.05.057>
- Delatycki, M. B. (2009). Evaluating the progression of Friedreich ataxia and its treatment. *Journal of Neurology*, 256(1), 36–41. <https://doi.org/10.1007/s00415-009-1007-y>
- Delatycki, M. B., & Corben, L. A. (2012). Clinical features of Friedreich ataxia. *Journal of Child Neurology*, 27(9), 1133–1137. <https://doi.org/10.1177/0883073812448230>
- Della Nave, R., Ginestroni, A., Diciotti, S., Salvatore, E., Soricelli, A., & Mascalchi, M. (2011). Axial diffusivity is increased in the degenerating superior cerebellar peduncles of Friedreich's ataxia. *Neuroradiology*, 53(5), 367–372. <https://doi.org/10.1007/s00234-010-0807-1>
- Della Nave, R., Ginestroni, A., Giannelli, M., Tessa, C., Salvatore, E., Salvi, F., ... Mascalchi, M. (2008). Brain structural damage in Friedreich's ataxia. *Journal of Neurology, Neurosurgery, and Psychiatry*, 79(1), 82–85. <https://doi.org/10.1136/jnnp.2007.124297>

- Della Nave, R., Ginestroni, A., Tessa, C., Salvatore, E., Bartolomei, I., Salvi, F., ... Mascalchi, M. (2008). Brain white matter tracts degeneration in Friedreich ataxia. An in vivo MRI study using tract-based spatial statistics and voxel-based morphometry. *NeuroImage*, 40(1), 19–25. <https://doi.org/10.1016/j.neuroimage.2007.11.050>
- Dogan, I., Tinnemann, E., Romanzetti, S., Mirzazade, S., Costa, A. S., Werner, C. J., ... Reetz, K. (2016). Cognition in Friedreich's ataxia: a behavioral and multimodal imaging study. *Annals of Clinical and Translational Neurology*, 3(8), 572–587. <https://doi.org/10.1002/acn3.315>
- Forman, S. D., Cohen, J. D., Fitzgerald, M., Eddy, W. F., Mintun, M. A., & Noll, D. C. (1995). Improved assessment of significant activation in functional magnetic resonance imaging (fMRI): use of a cluster-size threshold. *Magnetic Resonance in Medicine*, 33(5), 636–647. <https://doi.org/10.1002/mrm.1910330508>
- França, M. C., D'Abreu, A., Yasuda, C. L., Bonadia, L. C., Santos da Silva, M., Nucci, A., ... Cendes, F. (2009). A combined voxel-based morphometry and 1H-MRS study in patients with Friedreich's ataxia. *Journal of Neurology*, 256(7), 1114–1120. <https://doi.org/10.1007/s00415-009-5079-5>
- Georgiou-Karistianis, N., Akhlaghi, H., Corben, L. A., Delatycki, M. B., Storey, E., Bradshaw, J. L., & Egan, G. F. (2012). Decreased functional brain activation in Friedreich ataxia using the Simon effect task. *Brain and Cognition*, 79(3), 200–208. <https://doi.org/10.1016/j.bandc.2012.02.011>
- Gramegna, L. L., Tonon, C., Manners, D. N., Pini, A., Rinaldi, R., Zanigni, S., ... Lodi, R. (2017). Combined cerebellar proton MR spectroscopy and DWI study of patients with Friedreich's ataxia. *The Cerebellum*, 16(1), 82–88. <https://doi.org/10.1007/s12311-016-0767-z>
- Harding, I. H., Corben, L. A., Delatycki, M. B., Stagnitti, M. R., Storey, E., Egan, G. F., & Georgiou-Karistianis, N. (2017). Cerebral compensation during motor function in Friedreich ataxia: The IMAGE-FRDA study. *Movement Disorders*, 32(8), 1221–1229. <https://doi.org/10.1002/mds.27023>
- Harding, I. H., Corben, L. A., Storey, E., Egan, G. F., Stagnitti, M. R., Poudel, G. R., ... Georgiou-Karistianis, N. (2016). Fronto-cerebellar dysfunction and dysconnectivity underlying cognition in Friedreich ataxia: The IMAGE-FRDA study. *Human Brain Mapping*, 37(1), 338–350. <https://doi.org/10.1002/hbm.23034>
- Hatton, S. N., Panizzon, M. S., Vuoksima, E., Hagler, D. J., Fennema-Notestine, C., Rinker, D., ... Kremen, W. S. (2018). Genetic relatedness of axial and radial diffusivity indices of cerebral white matter microstructure in late middle age. *Human Brain Mapping*, 39(5), 2235–2245. <https://doi.org/10.1002/hbm.24002>
- Hua, K., Zhang, J., Wakana, S., Jiang, H., Li, X., Reich, D. S., ... Mori, S. (2008). Tract probability maps in stereotaxic spaces: analyses of white matter anatomy and tract-specific quantification. *NeuroImage*, 39(1), 336–347. <https://doi.org/10.1016/j.neuroimage.2007.07.053>
- Huang, J., Friedland, R. P., & Auchus, A. P. (2007). Diffusion tensor imaging of normal-appearing white matter in mild cognitive impairment and early Alzheimer disease: preliminary evidence of axonal degeneration in the temporal lobe. *American Journal of Neuroradiology*, 28(10), 1943–1948. <https://doi.org/10.3174/ajnr.A0700>
- Iltis, I., Hutter, D., Bushara, K. O., Clark, H. B., Gross, M., Eberly, L. E., ... Öz, G. (2010). 1H MR spectroscopy in Friedreich's ataxia and ataxia with oculomotor apraxia type 2. *Brain Research*, 1358, 200–210. <https://doi.org/10.1016/j.brainres.2010.08.030>
- Janve, V. A., Zu, Z., Yao, S.-Y., Li, K., Zhang, F. L., Wilson, K. J., ... Gochberg, D. F. (2013). The radial diffusivity and magnetization transfer pool size ratio are sensitive markers for demyelination in a rat model of type III multiple sclerosis (MS) lesions. *NeuroImage*, 74, 298–305. <https://doi.org/10.1016/j.neuroimage.2013.02.034>
- Jenkinson, M., Bannister, P., Brady, M., & Smith, S. (2002). Improved optimization for the robust and accurate linear registration and motion correction of brain images. *NeuroImage*, 17(2), 825–841. <https://doi.org/10.1006/nimg.2002.1132>
- Jones, D. K., Knösche, T. R., & Turner, R. (2013). White matter integrity, fiber count, and other fallacies: The do's and don'ts of diffusion MRI. *NeuroImage*, 73, 239–254. <https://doi.org/10.1016/j.neuroimage.2012.06.081>
- Keihaninejad, S., Zhang, H., Ryan, N. S., Malone, I. B., Modat, M., Cardoso, M. J., ... Ourselin, S. (2013). An unbiased longitudinal analysis framework for tracking white matter changes using diffusion tensor imaging with application to Alzheimer's disease. *NeuroImage*, 72, 153–163. <https://doi.org/10.1016/j.neuroimage.2013.01.044>
- Klauser, P., Baker, S. T., Cropley, V. L., Bousman, C., Fornito, A., Cocchi, L., ... Zalesky, A. (2017). White matter disruptions in schizophrenia are spatially widespread and topologically converge on brain network hubs. *Schizophrenia Bulletin*, 43(2), 425–435. <https://doi.org/10.1093/schbul/sbw100>
- Koeppen, A. H., Becker, A. B., Qian, J., & Feustel, P. J. (2017). Friedreich ataxia: Hypoplasia of spinal cord and dorsal root ganglia. *Journal of Neuropathology & Experimental Neurology*, 76(2), 101–108. <https://doi.org/10.1093/jnen/nlw111>
- Koeppen, A. H., & Mazurkiewicz, J. E. (2013). Friedreich ataxia: neuropathology revised. *Journal of Neuropathology & Experimental Neurology*, 72(2), 78–90. <https://doi.org/10.1097/NEN.0b013e31827e5762>
- Koeppen, A. H., Ramirez, R. L., Becker, A. B., Feustel, P. J., & Mazurkiewicz, J. E. (2015). Friedreich ataxia failure of GABA-ergic and glycinergic synaptic transmission in the dentate nucleus. *Journal of Neuropathology & Experimental Neurology*, 74(2), 166–176. <https://doi.org/10.1097/NEN.0000000000000160>
- Lecocq, C., Charles, P., Azulay, J.-P., Meissner, W., Rai, M., N'Guyen, K., ... Anheim, M. (2016). Delayed-onset Friedreich's ataxia revisited. *Movement Disorders*, 31(1), 62–69. <https://doi.org/10.1002/mds.26382>
- Lu, C., Schoenfeld, R., Shan, Y., Tsai, H.-J., Hammock, B., & Cortopassi, G. (2009). Frataxin deficiency induces Schwann cell inflammation and death. *Biochimica et Biophysica Acta (BBA)—Molecular Basis of Disease*, 1792(11), 1052–1061. <https://doi.org/10.1016/j.bbadis.2009.07.011>
- Martelli, A., & Puccio, H. (2014). Dysregulation of cellular iron metabolism in Friedreich ataxia: from primary iron-sulfur cluster deficit to mitochondrial iron accumulation. *Frontiers in Pharmacology*, 5, 130. <https://doi.org/10.3389/fphar.2014.00130>
- Mascalchi, M., Toschi, N., Giannelli, M., Ginestroni, A., Della Nave, R., Tessa, C., ... Diciotti, S. (2016). Regional cerebral disease progression in Friedreich's ataxia: a longitudinal diffusion tensor imaging study. *Journal of Neuroimaging*, 26(2), 130, 197–200. <https://doi.org/10.1111/jon.12270>
- Moghaddam, H. S., Sherbaf, F. G., & Aarabi, M. H. (2019). Brain microstructural abnormalities in type 2 diabetes mellitus: A systematic review of diffusion tensor imaging studies. *Frontiers in Neuroendocrinology*, 55, 100782. <https://doi.org/10.1016/j.yfrne.2019.100782>
- Oishi, K., Zilles, K., Amunts, K., Faria, A., Jiang, H., Li, X., ... Mori, S. (2008). Human brain white matter atlas: identification and assignment of common anatomical structures in superficial white matter. *NeuroImage*, 43(3), 447–457. <https://doi.org/10.1016/j.neuroimage.2008.07.009>
- Pagani, E., Ginestroni, A., Nave, R. D., Agosta, F., Salvi, F., Michele, G. D., ... Mascalchi, M. (2010). Assessment of brain white matter fiber bundle atrophy in patients with Friedreich ataxia. *Radiology*, 255(3), 882–889. <https://doi.org/10.1148/radiol.10091742>
- Pandolfo, M. (2008). Friedreich ataxia. *Archives of Neurology*, 65(10), 1296–1303. <https://doi.org/10.1001/archneur.65.10.1296>
- Parkinson, M. H., Boesch, S., Nachbauer, W., Mariotti, C., & Giunti, P. (2013). Clinical features of Friedreich's ataxia: classical and atypical phenotypes. *Journal of Neurochemistry*, 126(s1), 103–117. <https://doi.org/10.1111/jnc.12317>
- Poudel, G. R., Stout, J. C., Domínguez D, J. F., Churchyard, A., Chua, P., Egan, G. F., & Georgiou-Karistianis, N. (2015). Longitudinal change in white matter microstructure in Huntington's disease: The IMAGE-HD study. *Neurobiology of Disease*, 74, 406–412. <https://doi.org/10.1016/j.nbd.2014.12.009>

- Rausch, M., Tofts, P., Lervik, P., Walmsley, A., Mir, A., Schubart, A., & Seabrook, T. (2009). Characterization of white matter damage in animal models of multiple sclerosis by magnetization transfer ratio and quantitative mapping of the apparent bound proton fraction f . *Multiple Sclerosis Journal*, 15(1), 16–27. <https://doi.org/10.1177/1352458508096006>
- Rezende, T. J. R., Martinez, A. R. M., Faber, I., Girotto, K., Martins, M. P., de Lima, F. D., ... França, M. C. (2019). Developmental and neurodegenerative damage in Friedreich ataxia. *European Journal of Neurology*, 26(3), 483–489. <https://doi.org/10.1111/ene.13843>
- Rezende, T. J. R., Silva, C. B., Yassuda, C. L., Campos, B. M., D'Abreu, A., Cendes, F., ... França, M. C. (2016). Longitudinal magnetic resonance imaging study shows progressive pyramidal and callosal damage in Friedreich's ataxia. *Movement Disorders*, 31(1), 70–78. <https://doi.org/10.1002/mds.26436>
- Rizzo, G., Tonon, C., Valentino, M. L., Manners, D., Fortuna, F., Gellera, C., ... Lodi, R. (2011). Brain diffusion-weighted imaging in Friedreich's ataxia. *Movement Disorders*, 26(4), 705–712. <https://doi.org/10.1002/mds.23518>
- Rosas, H. D., Lee, S. Y., Bender, A. C., Zaleta, A. K., Vangel, M., Yu, P., ... Hersch, S. M. (2010). Altered white matter microstructure in the corpus callosum in Huntington's disease: Implications for cortical "disconnection". *NeuroImage*, 49(4), 2995–3004. <https://doi.org/10.1016/j.neuroimage.2009.10.015>
- Salat, D. H., Kaye, J. A., & Janowsky, J. S. (1999). Prefrontal gray and white matter volumes in healthy aging and alzheimer disease. *Archives of Neurology*, 56(3), 338–344. <https://doi.org/10.1001/archneur.56.3.338>
- Selvadurai, L. P., Harding, I. H., Corben, L. A., Stagnitti, M. R., Storey, E., Egan, G. F., ... Georgiou-Karistianis, N. (2016). Cerebral and cerebellar grey matter atrophy in Friedreich ataxia: the IMAGE-FRDA study. *Journal of Neurology*, 263(11), 2215–2223. <https://doi.org/10.1007/s00415-016-8252-7>
- Selvadurai, L. P., Harding, I. H., Corben, L. A., & Georgiou-Karistianis, N. (2018). Cerebral abnormalities in Friedreich ataxia: A review. *Neuroscience & Biobehavioral Reviews*, 84, 394–406. <https://doi.org/10.1016/j.neubiorev.2017.08.006>
- Smith, S. M. (2002). Fast robust automated brain extraction. *Human Brain Mapping*, 17(3), 143–155. <https://doi.org/10.1002/hbm.10062>
- Smith, S. M., Jenkinson, M., Woolrich, M. W., Beckmann, C. F., Behrens, T. E. J., Johansen-Berg, H., ... Matthews, P. M. (2004). Advances in functional and structural MR image analysis and implementation as FSL. *NeuroImage*, 23(Suppl. 1), S208–S219. <https://doi.org/10.1016/j.neuroimage.2004.07.051>
- Subramony, S. H., May, W., Lynch, D., Gomez, C., Fischbeck, K., Hallett, M., ... Ashizawa, T. (2005). Measuring Friedreich ataxia: Interrater reliability of a neurologic rating scale. *Neurology*, 64(7), 1261–1262. <https://doi.org/10.1212/01.wnl.0000156802.15466.79>
- Sun, S.-W., Liang, H.-F., Trinkaus, K., Cross, A. H., Armstrong, R. C., & Song, S.-K. (2006). Noninvasive detection of cuprizone induced axonal damage and demyelination in the mouse corpus callosum. *Magnetic Resonance in Medicine*, 55(2), 302–308. <https://doi.org/10.1002/mrm.20774>
- Tabrizi, S. J., Langbehn, D. R., Leavitt, B. R., Roos, R. A. C., Durr, A., Craufurd, D., ... Stout, J. C. (2009). Biological and clinical manifestations of Huntington's disease in the longitudinal TRACK-HD study: cross-sectional analysis of baseline data. *The Lancet Neurology*, 8(9), 791–801. [https://doi.org/10.1016/S1474-4422\(09\)70170-X](https://doi.org/10.1016/S1474-4422(09)70170-X)
- Tambasco, N., Nigro, P., Romoli, M., Simoni, S., Parnetti, L., & Calabresi, P. (2015). Magnetization transfer MRI in dementia disorders, Huntington's disease and parkinsonism. *Journal of the Neurological Sciences*, 353(1), 1–8. <https://doi.org/10.1016/j.jns.2015.03.025>
- van Baarsen, K. M., Kleinnijenhuis, M., Jbabdi, S., Sotiropoulos, S. N., Grotenhuis, J. A., & van Cappellen van Walsum, A. M. (2016). A probabilistic atlas of the cerebellar white matter. *NeuroImage*, 124, 724–732. <https://doi.org/10.1016/j.neuroimage.2015.09.014>
- Vavla, M., Arrigoni, F., Nordio, A., De Luca, A., Pizzighello, S., Petacchi, E., ... Martinuzzi, A. (2018). Functional and structural brain damage in Friedreich's ataxia. *Frontiers in Neurology*, 9, 747. <https://doi.org/10.3389/fneur.2018.00747>
- Verhoeven, K. J. F., Simonsen, K. L., & McIntyre, L. M. (2005). Implementing false discovery rate control: increasing your power. *Oikos*, 108(3), 643–647. <https://doi.org/10.1111/j.0030-1299.2005.13727.x>
- Vieira Karuta, S. C., Raskin, S., de Carvalho Neto, A., Gasparetto, E. L., Doring, T., & Teive, H. A. G. (2015). Diffusion tensor imaging and tract-based spatial statistics analysis in Friedreich's ataxia patients. *Parkinsonism & Related Disorders*, 21(5), 504–508. <https://doi.org/10.1016/j.parkreldis.2015.02.021>
- Ward, P. G. D., Harding, I. H., Close, T. G., Corben, L. A., Delatycki, M. B., Storey, E., ... Egan, G. F. (2019). Longitudinal evaluation of iron concentration and atrophy in the dentate nuclei in Friedreich ataxia. *Movement Disorders*, 34(3), 335–343. <https://doi.org/10.1002/mds.27606>
- Wheeler-Kingshott, C. A. M., & Cercignani, M. (2009). About "axial" and "radial" diffusivities. *Magnetic Resonance in Medicine*, 61(5), 1255–1260. <https://doi.org/10.1002/mrm.21965>
- Winkler, A. M., Ridgway, G. R., Webster, M. A., Smith, S. M., & Nichols, T. E. (2014). Permutation inference for the general linear model. *NeuroImage*, 92, 381–397. <https://doi.org/10.1016/j.neuroimage.2014.01.060>
- Yoon, S., Kim, J., Musen, G., Renshaw, P. F., Hwang, J., Bolo, N. R., ... Jacobson, A. M. (2018). Prefronto-temporal white matter microstructural alterations 20 years after the diagnosis of type 1 diabetes mellitus. *Pediatric Diabetes*, 19(3), 478–485. <https://doi.org/10.1111/pedi.12574>
- Zalesky, A., Akhlaghi, H., Corben, L. A., Bradshaw, J. L., Delatycki, M. B., Storey, E., ... Egan, G. F. (2014). Cerebello-cerebral connectivity deficits in Friedreich ataxia. *Brain Structure and Function*, 219(3), 969–981. <https://doi.org/10.1007/s00429-013-0547-1>
- Zhang, Y., Brady, M., & Smith, S. (2001). Segmentation of brain MR images through a hidden Markov random field model and the expectation-maximization algorithm. *IEEE Transactions on Medical Imaging*, 20(1), 45–57. <https://doi.org/10.1109/42.90642>

SUPPORTING INFORMATION

Additional supporting information may be found online in the Supporting Information section at the end of this article.

How to cite this article: Selvadurai LP, Corben LA, Delatycki MB, et al. Multiple mechanisms underpin cerebral and cerebellar white matter deficits in Friedreich ataxia: The IMAGE-FRDA study. *Hum Brain Mapp*. 2020;41:1920–1933. <https://doi.org/10.1002/hbm.24921>